JOURNAL OF MECHANICAL ENGINEERING, SCIENCE, AND INNOVATION
ITATS
Research Article

Quantum Mechanics Approach for Metal-Organic Frameworks Deformation Effect on Carbon Capture Performance: A Density Functional Theory Study

Journal of Mechanical Engineering, Science, and Innovation
e-ISNN: 2776-3536
2025, Vol. 5, No. 1
DOI: 10.31284/j.jmesi.2025.v5i1.7415
ejurnal.itats.ac.id/jmesi

Krisna Dwipa Muhdi[1] and Ahmad Atif Fikri[1]

[1]Department of Mechanical and Industrial Engineering, State University of Malang, Indonesia

Corresponding author:
Ahmad Atif Fikri
Department of Mechanical and Industrial Engineering, State University of Malang, Malang, 65145, Indonesia
Email: atif.fikri.ft@um.ac.id

Abstract

Increasing carbon dioxide (CO_2) emissions from fossil fuel combustion demand the development of effective and efficient carbon capture technologies. Metal-Organic Frameworks (MOFs) are excellent candidates as adsorbent materials because they have uniform pores, specific surface area, and can modified according to purpose. However, performance of MOFs may decrease due to structural deformation during adsorption-desorption process, especially under extreme conditions. This study uses a quantum mechanical approach, namely Density Functional Theory (DFT), to analyze effect of deformation, specifically hMOF-13, on its performance in CO_2 adsorption. Through modeling the atomic structure of hMOF-13, an understanding of the quantum interactions between atoms, changes in position of atoms and cells due to deformation is obtained. Simulation results show that mechanical deformation of hMOF-13 decreases CO_2 adsorption performance through pore narrowing and electrostatic charge redistribution. In addition, excessive deformation can trigger structural failures that reduce regeneration cycles and lower carbon capture efficiency. Insights from this study can guide the subsequent development of MOFs with enhanced mechanical resistance, contributing to the optimization of industrial-scale carbon capture processes. By improving the structural stability of MOFs, industries can achieve higher adsorption efficiency, longer material life, and reduced operational costs, making carbon capture technology more feasible and sustainable.

Keywords: *MOFs, Quantum Mechanics, Deformation, Density Functional Theory.*

Received: February 26, 2025; Received in revised: April 24, 2025; Accepted: April 26, 2025
Handling Editor: Afira Ainur Rosidah

INTRODUCTION

Rapid global energy demand and large-scale industry result in increasing greenhouse gas emissions, especially carbon dioxide (CO_2)[1]. More than 85% of global

energy demand depends on burning fossil fuels, which is the largest contributor to CO_2, so it is estimated that by 2050 CO_2 emissions will exceed 500 ppm, which is harmful to the environment and living things [2]–[3]–[4]. The unavoidable emission of CO_2 is a major cause of global warming, so CO_2 capture needs to be done. In addition to preventing global warming, CO_2 capture also plays a role in saving energy and raw materials for related industries, such as reducing CO_2 in natural gas to increase heating value and utilizing CO_2 for raw materials for making fertilizers [4]–[5]. This makes the development of effective carbon capture technology very urgent for the welfare of society and the sustainability of life [6].

CO_2 capture with solution-based adsorbents such as K_2SO_4 and zeolite membranes has been widely done, but carbon capture systems with these adsorbents require a large discharge and pressure that is relatively higher than atmospheric pressure to achieve efficient performance which results in greater energy use. This is because the percentage of CO_2 is smaller at 0.04% compared to other gases in the air such as nitrogen (N_2) which reaches 78%, oxygen (O_2) 30%, and argon (Ar) 0.90%, requiring a system that can capture a large air discharge to achieve efficient CO_2 capture [7]. A solution that can be done to reduce energy use in carbon capture is to use adsorbent materials that have high selectivity and adsorption capacity for CO_2. Metal-organic frameworks (MOFs) has been widely used because it has a uniform pore size and structure that can be adjusted and modified according to the intended use to capture a molecule in a gas such as CO2, in terms of energy consumption MOFs is also lower than solvent-based adsorbents [8]–[9]. The flexibility of MOFs to be modified provides the potential for the production of adsorbent materials that have high selectivity and adsorption capacity.

While MOFs possess advantages in selectivity and CO_2 adsorption capacity, its performance is highly dependent on their structural properties which could be reversible deformation during adsorption-desorption process. External pressures, gas-matter interaction, and the transition of thermodynamic conditions include temperature and humidity changes, cause this deformation. Morphological alterations are also observed in MOFs, including expansion and contraction of the pores, as have been documented to be responsible for diminishing adsorption capacity and altering selectivity towards the target gas [10]–[11]. Moreover, uncontrolled deformation also can accelerate the degradation of MOFs, decrease the regeneration cycle, and thus weaken the overall efficiency of the carbon capture system [12]. Due to the complexity in MOF structure and behavior change as well, particularly for CO_2 capture, a Quantum Mechanics (QM) based approach is needed to understand the deformation mechanism and explore transformation impact on MOF performance. Traditional methods like force field molecular dynamics or macroscopic approaches often do not account for changes in electronic properties and complex quantum power interactions in MOFs systems.

QM is derived from the Schrödinger equation characterizing the ground state of quantum mechanical systems. However, solving the Schrödinger equation exactly for many-electron systems is challenging, due to the correlation between the coordinates of electrons arising from these interactions in the wave function. This problem to find a solution of Schrödinger equation for many electron system is addressed by Density Functional Theory (DFT) that states the wave function of a system can be represented as a function of electron density having a capability of calculation according to Hohenberg-Kohn theory [13]. Therefore, the QM approach and even the DFT method can give much more insight into interactions between atoms in many-electron MOFs, mechanism of CO_2 adsorption on active sites, and energy changes resulting from structural deformation [14]–[15]. For carbon capture applications, the quantum mechanical-based analysis can be exploited and more accurately assessed in relation to key parameters including bonding energy, charge distribution, bonding force and the structural response under

external pressure which in turn lead to more optimized design and modifications of MOFs [16]–[17].

Quantum Mechanic Function

The Schrödinger equation as one of the basic functions on a quantum scale can be an approach solution to determine the electron density of an atom. Electron density can affect the physical and chemical properties of compounds, including bond length, polarity, and bond energy, so that in MOF materials, electron density determines the interaction of MOF molecules with guest molecules which can affect the adsorption ability of MOF molecules [18]. The Schrödinger wave function is shown in Equation (1).

$$\hat{H}\psi(r1, r2, \ldots, rn) = E\psi(r1, r2, \ldots, rn) \quad (1)$$

Where, $\hat{H}$ is the total Hamilton of the system consisting of the kinetic energy of the electrons, the ectsernal potential interaction of the atomic nucleus, and the Coulomb interaction between electrons. Ψ is a wave function with many electrons and E is the total energy of the system. Energy in the atom consists of three components namely, kinetic energy (E_k), Hartree energy (E_H), and exchange energy (E_X) which are defined in the form of a single particle state (φ_a) [18], shown in Equation (2) to Equation (4).

$$E_k = \sum_a v_\alpha^2 \int dr\, \bar{\varphi}[-i\gamma\nabla + M]\varphi_a \quad (2)$$

$$E_H = \frac{1}{2}\sum_{\phi;ab} v_a^2\, v_b^2 \iint dr\, dr' \left[\bar{\varphi}_a \Gamma_\phi \varphi_a\right]_r D_\phi(rr') \left[\bar{\varphi}_b \Gamma_\phi \varphi_b\right]_{r'} \quad (3)$$

$$E_x = -\frac{1}{2}\sum_{\phi;ab} v_a^2\, v_b^2 \iint dr\, dr' \left[\bar{\varphi}_a \Gamma_\phi \varphi_a\right]_r D_\phi(rr') \left[\bar{\varphi}_b \Gamma_\phi \varphi_b\right]_{r'} \quad (4)$$

Where, M is the mass of the nucleon, v_α^2 is the occupancy probability, Γ_ϕ and D_ϕ is the interaction vertex and propagator, respectively, with ϕ is meson σ, ω, ρ, and the interacting photon A in the effective Lagrangian. The important thing in the equation is E_k and E_x is an orbital-dependent functional and E_H represented as a functional of the scalar density ρ_s and current vector j^μ, with τ represents neutrons in protons [13], as in Equation (5) and Equation (6).

$$\rho_s, \tau = \sum_{a\in\tau} v_a^2\, \bar{\varphi}_a(r)\varphi_a(r) \quad (5)$$

$$j_s^\mu = \sum_{a\in\tau} v_a^2\, \bar{\varphi}_a(r)\varphi_a(r) \quad (6)$$

The adsorbent material selected for this study is hMOF-13, chosen for its relatively higher CO_2 loading capacity compared to other MOFs, while exhibiting lower N_2 loading. This property gives hMOF-13 a strong selectivity for CO_2 capture from ambient air, which is predominantly composed of nitrogen [19]. In addition, hMOF-13 demonstrates good pressure stability, enabling more efficient and effective adsorption–desorption processes across a variety of carbon capture scenarios [20]. The prefix "h" in hMOF-13 stands for "hypothetical", indicating that the structure has not been synthesized experimentally, but was generated through computational modeling and simulation. Such structures are typically developed for predictive studies involving the adsorption of gases such as carbon dioxide, methane, and others. The number "13" refers to the entry index of this material in the MOFXDB API database, a validated data source that has been published in the *Journal of Chemical & Engineering Data*, Volume 68, Issue 2, by the American Chemical Society (ACS Publications).

METHODS AND ANALYSIS

This research focuses on the effects of geometry changes that occur in hMOF-13 on

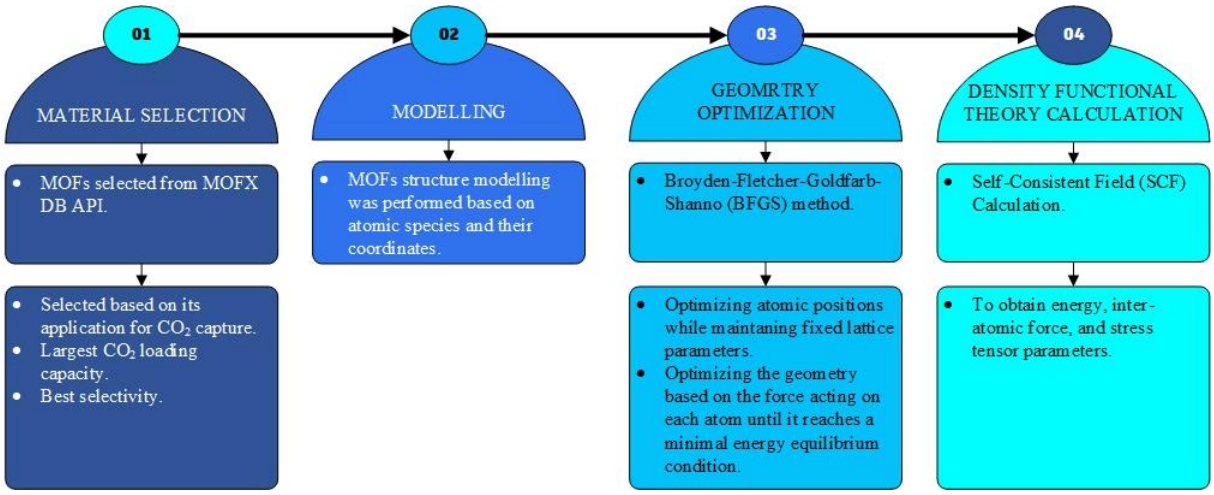

Figure 1. Research flow.

Table 1. Propertise of hMOF-13 [20].

No.	Propertise	Value
1	Void Fraction	0.359167
2	Accessible Surface Area (ASA) (m^2/g) / (m^2/cm^3)	486.4/626.6
3	Pore Limiting Diameter (PLD) (Å)	3.250
3	Largest Cavity Diameter (LCD) (Å)	4.250
5	Atoms in MOF	Zn, O, C, H. F
6	Atomics Mass of Cell	1611.7
7	Cif Volume ($Å^3$)	2077.260
8	CO_2 Loading Capacity (mol/kg), at 0.5 bar	5.691
9	N_2 Loading Capacity (mol/kg), at 0.9 bar	0.146
10	CO_2 Heat of Adsoprtion (kj/mol), at 0.05-0.5 bar	35.917-35.939
11	N_2 Heat of Adsoprtion (kj/mol), at 0.09-0.9 bar	18.245-18.348

parameters that affect CO_2 capture performance, the flow of this research is shown in Figure 1.

The selection of the MOF in this study was based on three primary criteria: its applicability in carbon dioxide capture particularly for direct air capture (DAC) processes its high CO_2 loading capacity, as indicated by simulation data at specific partial pressures, and its strong selectivity toward CO_2 over other gases such as N_2. This selectivity is essential for efficiently separating CO_2 from nitrogen-rich air [20]. Among the evaluated candidates, hMOF-13 was selected, as it demonstrated the most favorable combination of these three criteria based on the simulation results. The following hMOF-13 property data is shown in Table 1.

Broyden-Fletcher-Goldfarb-Shanno (BFGS) Method

Geometry optimization aims to find an atomic configuration that has the minimum total energy, i.e. when the force on each atom is close to zero. This is done by moving atoms little by little following an energy gradient until the system reaches structural equilibrium. Geometry optimization is performed using the Broyden-Fletcher-Goldfarb-Shanno (BFGS) Method based on the quasi-Newton algorithm [21]. This method is used to avoid direct computation of the Hessian by building an approximation of the Hessian matrix iteratively based on changes in atomic forces and positions during optimization. The working principle of BFGS is by defining changes in atomic position and force changes against the energy gradient, then the approximation of the Hessian matrix will be updated

and go to a new step until the condition converges based on the energy convergence limit to be achieved [22], which is expressed by Equation (7).

$$H_{k+1} = \left(I - \frac{S_k y_k^T}{y_k^T S_k}\right) H_k \left(I - \frac{y_k S_k^T}{y_k^T S_k}\right) + \frac{S_k S_k^T}{y_k^T S_k} \quad (7)$$

Where, H_k represents the inverse Hessian approximation at iteration k, I is the identity matrix, S_k denotes the change in position $x_{k+1} - x_k$, and y_k refers to the change in gradient $g_{k+1} - g_k$. This equation efficiently updates the inverse Hessian without the need to explicitly compute second derivatives. The resulting matrix is then used to determine the direction of atomic position updates for the next iteration [22].

Density Functional Theory

Hohenberg-Kohn states that all basic properties of systems with many electrons can be determined from the electron density, so there is no need to know the wave function of many-electron systems explicitly [13]. which is expressed by Equation (8).

$$\rho_r \rightarrow \begin{Bmatrix} v[\rho(r)] \\ N[\rho(r)] \end{Bmatrix} \rightarrow \hat{H}[\rho(r)] \rightarrow \{\psi_i[\rho(r)]\} \quad (8)$$

Where i= (0, 1, 2, …., ∞)refers to the electron state. Then to calculate the many-electron interaction the Kohn-Sham equation is used by integrating the exact exchange energy for the nucleus with arbitrary deformation using the inverse Hamiltonian and the spectral method [13]–[18], which is shown in Equation (9).

$$\hat{h} = -i\alpha\nabla + \beta\left[M + S_\tau(r) + \gamma_\mu V_\tau^\mu(r)\right] \quad (9)$$

Where $\hat{h}$ is the single particle Hamiltonian. Note that S_τ and V_τ is a local potential derived from the variation of the energy functional, which can be further divided into Hartree and exchange components. Hartree potential $S_\tau(r)$ dan $V_\tau^\mu(r)$ can be obtained by calculating the density and current that represent the coulumb interaction between electrons as shown in Equation (10) and Equation (11) [18].

$$S_\tau(r) = S_{H,\tau}(r) + S_{X,\tau}(r) = \frac{\delta E_H}{\delta \rho_{s,\tau}} + \frac{\delta E_X}{\delta \rho_{s,\tau}} \quad (10)$$

$$V_\tau^\mu(r) = V_{H,\tau}^\mu(r) + V_{X,\tau}^\mu(r) = \frac{\delta E_H}{\delta (j_\tau)_\mu} + \frac{\delta E_X}{\delta (j_\tau)_\mu} \quad (11)$$

The exchange-correlation potential that fixes the many-electron interaction has a more complex approach, which is calculated in the non-interacting approach and is an independent electron wave function (dependent on the Kohn-Sham orbit) that represents the analog of the one-electron Schrödinger wave function represented in Equation (12). and Equation (13) [18].

$$S_{x,\tau}\rho_{s,\tau} + V_{x,\tau}^v(j_\tau)_v = \frac{1}{2}\sum_{a\in\tau} v_a^2 \{\bar{\varphi}_a(W_a - \zeta_a\gamma^0)\varphi_a + c.c\} \quad (12)$$

$$S_{x,\tau}j_{x,\tau}^\mu + V_{x,\tau}^v\rho_{s,\tau} = \frac{1}{2}\sum_{a\in\tau} v_a^2 \{\bar{\varphi}_a(W_a - \zeta_a\gamma^0)\gamma^\mu\varphi_a + c.c\} \quad (13)$$

Where W_a is the orbital specific potential $W_a = \frac{\bar{\phi}_a}{\delta\phi_a}$ and ζ_a is the energy shift. The total energy in the system is obtained from the sum of kinetic energy (E_K), Hartree energy (E_H), and exchange-correlation energy (E_X) which [18], is represented in Equation (14).

$$E_{total} = E_k + E_H + E_x \quad (14)$$

The bonding forces in the hMOF-13 structure are calculated from the total energy gradient against the atomic coordinates obtained from the derivative of the total potential energy against the atomic positions in the system as in Equation (15).

$$F_i = \frac{\partial E_{total}}{\partial R_i} \quad (15)$$

Where, F_i is the force on the atom i, ∂R_i is atom position i, dan ∂E_{total} which is the total energy in the system. An analysis of the stability and dynamics of the system needs to be carried out to determine the interaction of h-MOF-13 with elements in the air. Approach with Potential Energy Surface (E_{PES}) as in Equation (16). can describe the variation of total energy against changes in the initial atomic position (E_0) in the system if the hMOF-13 structure is deformed so that the stability and dynamics of the system can be analyzed [23].

$$E_{PES} = E_{total}(R_1, R_2, \ldots . R_n) - E_0 \quad (16)$$

$$E_B = E_{PL} - E_g - E_{ads} \quad (17)$$

In addition to calculating the energy for the CO2 capture process, the energy to release CO2 from the hMOF-13 membrane is also important to calculate. The energy that affects the release process is binding energy which is a measure of the energy required to separate the system into its individual fragments, in this case separating the CO2 molecule from the hMOF-13 structure molecule. Binding energy (E_B) represented as a calculation of the total system energy (EPL) minus the total adsobernt energy (E_g) and the total energy (E_{ads}) of the molecule to be captured, namely CO2 in free conditions without interaction between the two [24], as shown in Equation (16). The Lennard-Jones potential is used to describe the van der waals forces between MOF atoms [13], which is represented in Equation (18).

$$U_{LJ}(r) = 4\epsilon \left[\left[\frac{\sigma^{12}}{r}\right]\right] - \left[\left[\frac{\sigma^{6}}{r}\right]\right] \quad (18)$$

Where, ϵ is the minimum depth of potential energy, σ is the distance at which the potential energy is zero, and r is the distance between atoms. Since hMOF-13 often has charged groups such as coordinated metals or polar functional groups, it is important to calculate electrostatic interactions [25].

$$U_{Coulomb}(r) = \frac{1}{4\pi\epsilon_0}\frac{(q_1 q_2)}{r} \quad (19)$$

The Coulomb potential can be used to describe these electrostatic interactions [13], Where q1 and q2 is the charge of two particles, as in Equation (19).

This study employed calculations based on Equations 10 through 19, which serve as the functional components within Density Functional Theory (DFT). The DFT equations are founded on the Hohenberg–Kohn theorem, which states that the properties of a many-electron system can be determined solely from its electron density, without the need to explicitly express the many-body wave function as required in Schrödinger's theory. This is particularly suitable for modeling complex structures like hMOF-13, which contains millions of electrons. These equations have also been adopted in several previous studies [18]–[25].

The software used for the BFGS optimization and DFT calculations in this study is Quantum ESPRESSO (QE). QE is a widely used open-source software package based on DFT, designed for simulating the electronic structure of materials at the atomic scale. The initial settings for both the BFGS and DFT simulations are provided in the Supplementary

Table 2. Boundary Conditions

No.	Boundary Conditions Parameters	Value
1	Convergence Threshold	1×10^{-6}
2	k-Point Mesh	$1\times 1\times 1$
3	Cutoff Energy Wave Function (Ry	50.0
4	Cutoff Energy Rho (Ry)	200.0
5	Electron Maxstep	100
6	Pressure (kbar)	0.001-1
7	Temperature (K)	305

File.

Type of calculation applied in the DFT simulation was the Self-Consistent Field (SCF) method, which aims to obtain the total energy of the system, interatomic forces, and stress–strain parameters resulting from structural deformation. The information obtained from the SCF calculation is then used to evaluate the response of the MOF structure to external pressure and its impact on CO_2 adsorption performance.

Boundary Conditions

The definition of boundary conditions and atomic structure modeling of hMOF-13 were conducted to support geometry optimization using the BFGS method and subsequent DFT calculations. The modeling was based on the atomic species (such as Zn, O, C, H, and F) and their positional coordinates, which were obtained from the Crystallographic Information File (CIF) available in the database, as shown in the Supplementary File. The structure was constructed in the form of a supercell to simulate the periodic nature of the material. The aim of this stage was to prepare a representative initial system for geometry optimization and DFT analysis. The applied boundary conditions are listed in Table 2.

The convergence criterion for the DFT simulations in this study was defined as reaching a minimum total energy of 1×10^{-6} Ry before the electron_maxstep value reaches 100. The electron_maxstep parameter represents the maximum number of iterative steps allowed in the self-consistent solution process for the wave function and electron density. If this threshold is exceeded without achieving convergence, the algorithm terminates and considers the calculation non-convergent.

RESULTS AND DISCUSSIONS

Material Modelling

hMOF-13 obtained from the MOFX-DB database [20], was modeled to describe its structure. hMOF-13 has a repeating structure with metal nodes and organic linkers as the main components. Metal atoms consist of zinc (Zn) and organic atoms consist of oxygen (O), carbon (C), hydrogen (H), and fluorine (F). Thus, this structure allows MOFs to have high porosity, large specific surface area, and selective ability to capture and store gases such as CO_2 [26]–[17]. The structure of hMOF-13 is shown in Figure 2.

Zn in hMOF-13 functions as a coordination center (metal node) that connects organic ligands through interactions with oxygen. Zn has high electropositive properties, so it can form strong coordination bonds with functional groups such as carboxylates ($-COO^-$). The role of Zn in CO_2 adsorption is also significant, as it can contribute to electrostatic interactions that increase the selectivity and efficiency of gas capture [27]. O in the MOFs structure acts as a bridge connecting Zn with organic ligands. The presence of oxygen not only strengthens structural stability, but also plays a role in the formation of hydrogen bonds, which are important in enhancing the interaction between MOFs and CO_2 [28].

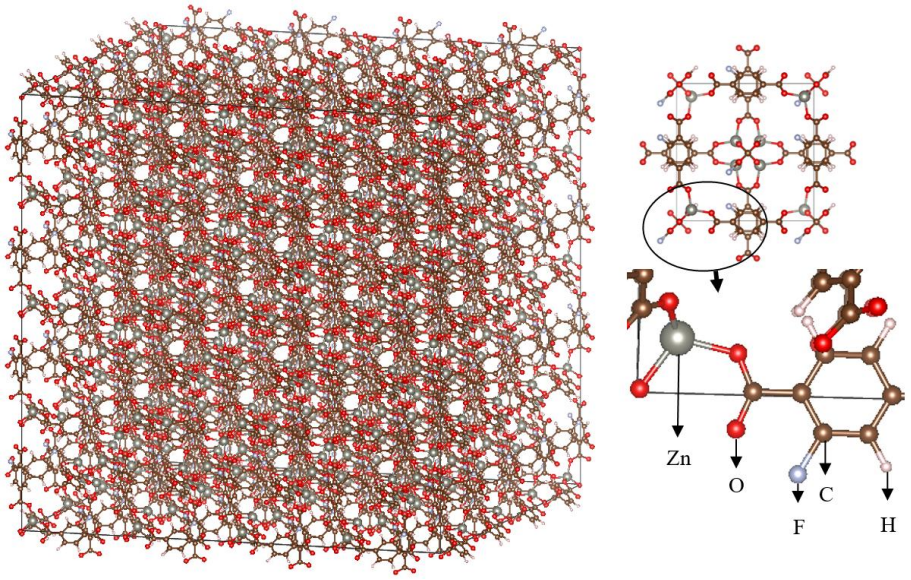

(a) (b)

Figure 2. (a) Super cell hMOF-13 and (b) Atom composition hMOF-13.

C is the main component in the organic ligands that make up the MOF series. Carbon-based ligands usually contain aromatic groups or carbon chains that can enhance interactions π-stacking with CO_2, mainly through van der Waals forces or electrostatic interactions [29]. Flexible ligands allow the MOFs structure to adjust to external stresses, thereby increasing its adsorption capacity. In addition, the presence of H in the MOFs structure also plays a role in hydrogen bonding interactions, which can strengthen the stability of the structure and affect the polarity of the MOF. These hydrogen bonding interactions often play a role in gas capture selectivity, especially in environments with gas mixtures such as CO_2 and H_2O [30]. The presence of F in the MOF structure can have unique effects, especially in terms of surface modification and hydrophobic properties. Fluorine groups are often used to improve water resistance, so MOFs remain stable under high humidity conditions. In addition, fluorine can also affect the adsorption energy of CO_2 by modifying the electrostatic interaction and polarity of MOFs, thereby increasing the adsorption selectivity towards CO_2 compared to other gases [31].

Metal-Organic Framework Failure

Mechanical simulation of the hMOF-13 cell structure was carried out at pressures of 0.001 kbar to 1 kbar in a temperature of 305 K to see the response of hMOF-13 to the extreme external forces that occur. The applied pressure conditions represent a range from normal atmospheric environments to extreme scenarios in carbon capture applications, allowing observation of structural changes experienced by hMOF-13 under excessive pressure.

Based on the simulation results, the maximum stress experienced by hMOF-13 is 3.642×10^{-6} Ry/bohr^3, with a maximum strain before structural failure of 0.91×10^{-7} Å/Å. The stress-strain relationship graph shows an elastic response at an early stage, where an increase in strain leads to a linear increase in stress. However, at a critical strain value 0.91×10^{-7} Å/Å, stress reaches a maximum before decreasing, signaling plastic deformation and the beginning of structural failure.

Structural failures in Metal-Organic Framework (MOF) materials occur due to CO2 adsorption and external forces that cause changes in the atomic coordination network and inter-molecular interactions. In the case of hMOF-13, these failures mainly depend on the values of van der Waals interactions and electrostatic (Coulombic) forces that play an important role in the stability of the framework. At low pressures which is worth 0.001 kbar, van der Waals interactions between ligands and Zn coordination centers are still strong enough to maintain the stability of the network. The structure of hMOF-13 remains

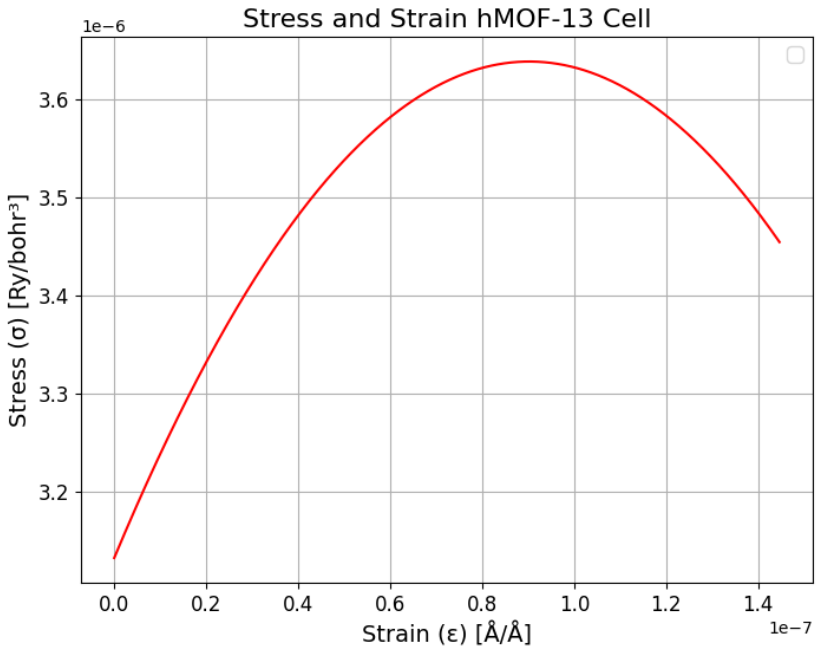

Figure 3. Strutukr cell hMOF-13 failure chart

porous and does not undergo significant changes apart from a slight shift in atomic positions due to thermal energy fluctuations [32]. However, as the pressure increases to 0.1 kbar, the Zn-O coordination network starts to deform, leading to slight changes in the cell volume and lattice parameters. However, at this stage, the coordination interaction between Zn and the organic ligand is still strong enough to maintain the overall framework shape.

At high pressures of 1 kbar, van der Waals forces are no longer strong enough to resist deformation, resulting in greater atomic drift and potential framework collapse. At this stage, charge redistribution occurs due to changes in atomic positions, which directly affects the Coulombic interactions in the system [33]. When the strain reaches a critical value 0.91×10^{-7} Å/Å, electrostatic forces between atoms become unstable as the charge balance is disrupted, leading to a weakening of the forces of attraction between ligands and the Zn coordination center. As a result, the structure experiences a drastic change in potential energy, which marks the beginning of mechanical failure.

Deformation Effects on CO_2 Capture Performance

The structural failure experienced by hMOF-13 has a significant impact on CO_2 adsorption capacity, mainly due to changes in pore geometry and electrostatic charge distribution as shown in Figure 4. One of the main effects is the reduction in effective surface area, where the deformation that occurs results in pore narrowing and a reduced number of active adsorption sites. This inhibits the diffusion of CO_2 into the framework, thus reducing the gas storage capacity [34]. The values of the change in total energy and structure of hMOF-13 are shown in Table 3.

The variations in Van der Waals forces observed in the simulation results do more than illustrate the strength of interatomic interactions they also play a direct role in shaping the adsorption energy of MOF materials. In frameworks such as hMOF-13, the adsorption energy of CO_2 is significantly influenced by both the depth and stability of the potential energy landscape governing atom-to-atom interactions. This behavior is largely represented by the parameter ε in the Lennard-Jones Equation (18).

A higher ε value, as seen in Zn–O atom pairs, indicates a stronger attractive force, which is ideal for retaining CO_2 molecules within the porous network during the adsorption process. However, when structural deformation alters the distance between

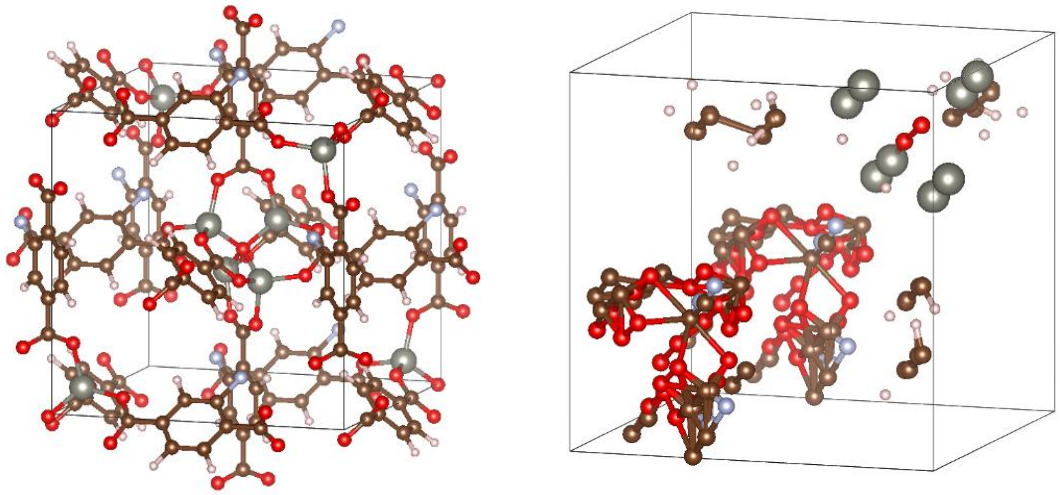

a. **b.**

Figure 4. Cell structure of hMOF-13, (a) Before deformation and (b) After deformation, at pressures of 0.001 kbar to 1kbar.

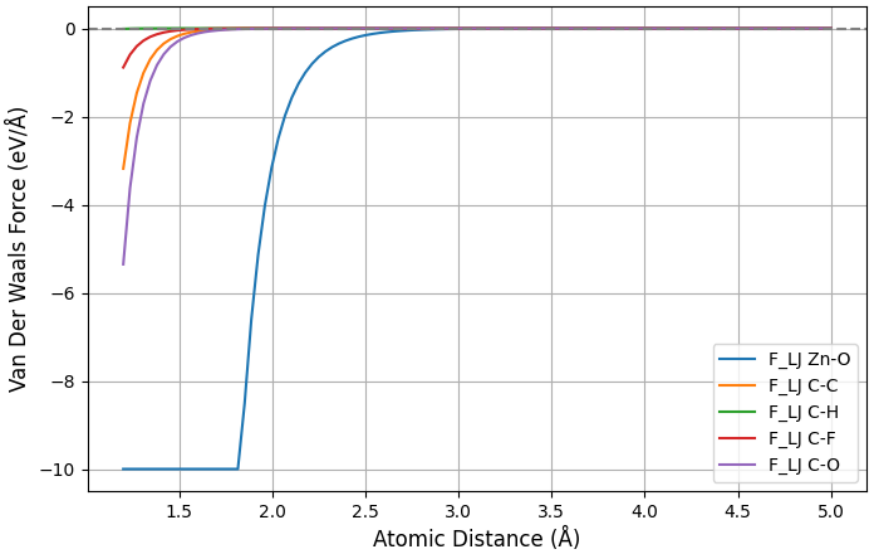

Figure 5. Van Der Waals forces on hMOF-13 at pressures of 0.001 kbar to 1kbar.

Table 3. Change value of energy and cell structure of hMOF-13

Parameters	Before Deformation	After Deformation
Total Energy	-2089.584280293659	-2089.584078418853
Cell lengths		
a (Å)	24.111773	24.111775
b (Å)	24.111770	24.111774
c (Å)	24.111759	24.111763
Cell angles		
α (°)	89.970040	89.970013
β (°)	89.979946	89.979899
γ (°)	90.013696	90.013715

atoms either by bringing them too close, resulting in repulsive forces, or by pushing them too far apart, weakening the interaction the adsorption energy is also affected. In this study, the data reveal that as pressure increases and structural deformation intensifies,

Van der Waals forces become increasingly unstable and decline exponentially. This trend leads to a measurable drop in the net adsorption energy (binding energy), as the material becomes less effective in anchoring CO_2 molecules within its framework [35].

Put simply, greater deformation corresponds to lower adsorption energy due to the increasingly suboptimal interaction between the MOF structure and the gas molecules. This reduction in energetic affinity ultimately lowers CO_2 capture efficiency, especially under conditions involving high pressure or repeated adsorption-desorption cycles in industrial environments. Therefore, maintaining the structural integrity and atomic interaction parameters of the MOF is essential for ensuring consistently high adsorption energy and overall capture performance [36].

The Coulomb potential graph in Figure 6 shows the electrostatic relationship between pairs of atoms in hMOF-13. This electrostatic potential arises from the interaction between the partial charges of two atoms, q1 and q2, separated by a distance r. In Figure 6, it can be seen that the interaction between Zn-O has a significant negative potential value, indicating a strong electrostatic attractive force between positively charged Zn and negatively charged O. In contrast, interactions such as C-O, C-C, and C-F show smaller positive potential values, indicating an electrostatic interaction between the positively charged Zn and negatively charged O. In contrast, interactions such as C-O, C-C, and C-F show smaller positive potential values, signaling weaker or even repulsive electrostatic interactions in some cases [37].

As the distance between atoms increases, the Coulomb potential gradually decreases towards zero, as described in the Coulomb Equation (18). This shows that at larger distances, the electrostatic force becomes weaker, so the interaction between atoms becomes less significant. When deformation causes the distance between atoms to

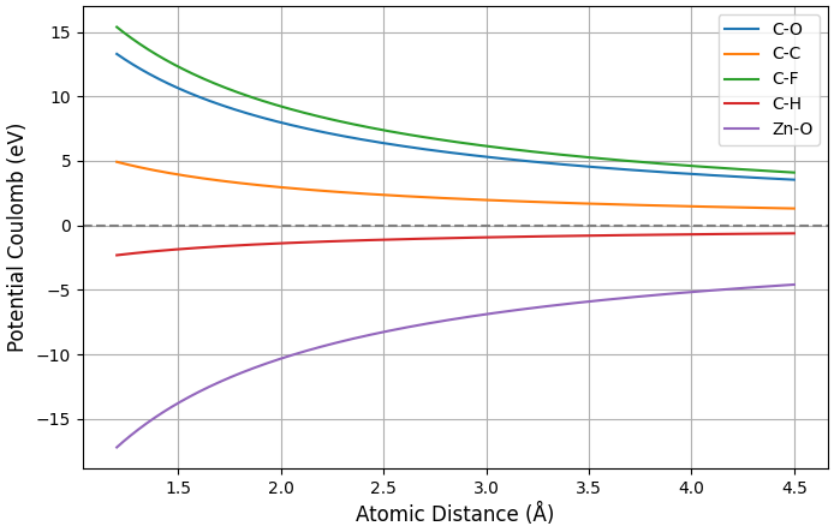

Figure 6. Coulomb interaction on hMOF-13 at pressures of 0.001 kbar to 1kbar.

Table 4. Changes in atomic position due to deformation

Parameters	Largest change in atomic position	Smallest change in atomic position
Atom to	66	80
Atom Species	C	C
dX (Å)	46.641	46.652
dY (Å)	-0.146	-0.134
dZ (Å)	-9.178	6.162
Total Displacement (Å)	47.536	47.057

shrink, the electrostatic forces can increase significantly, potentially leading to structural instability due to excessive attraction or repulsion forces. Conversely, if the structure undergoes expansion, the electrostatic interaction weakens, which may reduce the cohesion in the MOF network and affect the mechanical properties as well as the adsorption of hMOF-13 [38]. Thus, the calculation of Coulomb potential is important to understand the material response to deformation as well as to design MOFs with optimal electrostatic stability to enhance the adsorption of MOFs to the gas to be captured. Changes in atomic positions due to deformation are shown in Table 4.

These structural failures also have implications for the durability of MOFs under repeated pressure cycles. In industrial applications such as gas storage and separation, MOFs are subjected to repeated gas charging and discharging cycles. If the framework undergoes permanent deformation due to external pressure, the porosity and CO_2 adsorption capacity will decrease over time [39]. This indicates that the mechanical stability of hMOF-13 should be a major concern in material design for gas storage applications under operational conditions involving high pressure.

This study provides significant practical insights into the development of MOF-based CO_2 capture systems under industrially relevant conditions. Through quantum mechanical simulations using Density Functional Theory (DFT), it was revealed that while hMOF-13 maintains structural integrity at low to moderate pressures, it suffers from structural collapse at higher pressures due to geometric deformation, pore narrowing, and electrostatic charge redistribution. These phenomena directly reduce CO_2 adsorption capacity and material regeneration performance.

The findings highlight that the performance of MOFs in CO_2 capture is not solely dependent on isothermal adsorption data, but also on their mechanical resilience under cyclic operational stresses. This underlines the necessity for rational material design that incorporates pressure-resistance considerations. Three strategies are proposed to enhance MOF durability and efficiency in real applications: (i) ligand modification to improve framework flexibility, (ii) incorporation of stronger electrostatic interactions through polar functional groups or ionic moieties, and (iii) reinforcement of metal-ligand coordination, particularly the Zn–O network, to prevent collapse under high pressure.

These results offer a theoretical foundation for the pre-screening of MOF candidates before synthesis, allowing researchers to identify and tailor materials with optimized structural stability and high selectivity for CO_2 capture. By addressing the structural failure mechanisms at the atomic scale, this study contributes to the design of next-generation MOFs with enhanced lifespan, lower operational costs, and improved adsorption performance in industrial carbon capture technologies.

CONCLUSIONS

This study confirms the critical role of structural deformation in influencing the performance of hMOF-13 for CO_2 capture. By applying Density Functional Theory (DFT), the research provides a detailed understanding of how changes in lattice parameters and electron density redistribution impact the interaction between the material and CO_2 molecules. The simulation results indicate that high-pressure conditions lead to pore constriction and a reduction in active adsorption sites, ultimately diminishing CO_2 storage capacity. Furthermore, atomic displacement and the resulting charge imbalance weaken the electrostatic interactions crucial for selective gas capture. These findings underscore the importance of mechanical stability and structural design in the development of MOF-based materials for industrial applications, particularly under cyclic and high-pressure operating environments. Strategies such as ligand modification, reinforcement of metal-ligand coordinationespecially the Zn–O network and the introduction of polar functional groups are suggested to enhance structural durability and maintain optimal adsorption capacity.

Looking ahead, future studies could expand this quantum mechanical approach to investigate other MOF variants with different topologies and chemical compositions. In addition, integrating machine learning (ML) and artificial intelligence (AI) techniques into the screening process offers a promising pathway to accelerate the discovery and optimization of high-performance MOFs. By combining atomistic simulations with predictive modeling, this research lays the groundwork for designing next-generation MOFs that are not only efficient but also robust under real-world operating conditions.

ACKNOWLEDGEMENTS

The authors gratefully acknowledge the help of colleagues who contributed to this research.

DECLARATION OF CONFLICTING INTERESTS

The authors declare that there are no potential conflicts of interest related to the research described in the publication of this article.

FUNDING

Thank you to PT ARJUNA ADI MAKMUR for supporting and facilitating this research.

REFERENCES

[1] X. Cheng, Y. Liao, Z. Lei, et al., "Multi-scale design of MOF-based membrane separation for CO2/CH4 mixture via integration of molecular simulation, machine learning and process modeling and simulation," *J. Memb. Sci.*, vol. 672, no. July 2022, p. 121430, 2023, doi: 10.1016/j.memsci.2023.121430.

[2] A. A. Fikri, I. Fadlika, A. N. Saeful, et al., "Heuristic Approach to Comparing the Environmental Impacts of Carbon Nanotube Production Methods," *J. Mech. Eng. Sci. Technol.*, vol. 8, no. 1, pp. 199–214, 2024, doi: 10.17977/um016v8i12024p199.

[3] A. M. Yousef, W. M. El-Maghlany, Y. A. Eldrainy, et al., "New approach for biogas purification using cryogenic separation and distillation process for CO2 capture," *Energy*, vol. 156, pp. 328–351, 2018, doi: 10.1016/j.energy.2018.05.106.

[4] F. Chen *et al.*, "Carbon dioxide capture in gallate-based metal-organic frameworks," *Sep. Purif. Technol.*, vol. 292, no. March, p. 121031, 2022, doi: 10.1016/j.seppur.2022.121031.

[5] M. A. Morales Mora, C. P. Vergara, M. A. Leiva, et al., "Life cycle assessment of carbon capture and utilization from ammonia process in Mexico," *J. Environ. Manage.*, vol. 183, pp. 998–1008, 2016, doi: 10.1016/j.jenvman.2016.09.048.

[6] Y. J. Park, S. Yoon, and S. E. Jerng, "Machine learning of metal-organic framework design for carbon dioxide capture and utilization," *J. CO2 Util.*, vol. 89, no. September, p. 102941, 2024, doi: 10.1016/j.jcou.2024.102941.

[7] S. K. Shivaranjani and A. Gandhimathi, "Analysis and assessment of gaseous pollutants along high traffic roads (NH 948) in Coimbatore city, India," *Glob. Nest J.*, vol. 25, no. 10, pp. 102–109, 2023, doi: 10.30955/gnj.005181.

[8] J. Hu, Y. Liu, J. Liu, et al., "Computational Screening of Alkali, Alkaline Earth, and Transition Metals Alkoxide-Functionalized Metal-Organic Frameworks for CO2 Capture," *J. Phys. Chem. C*, vol. 122, no. 33, pp. 19015–19024, 2018, doi: 10.1021/acs.jpcc.8b05334.

[9] T. D. Burns *et al.*, "Prediction of MOF Performance in Vacuum Swing Adsorption Systems for Postcombustion CO2 Capture Based on Integrated Molecular Simulations, Process Optimizations, and Machine Learning Models," *Environ. Sci. Technol.*, vol. 54, no. 7, pp. 4536–4544, 2020, doi: 10.1021/acs.est.9b07407.

[10] S. Parshamoni, S. Sanda, H. S. Jena, et al., "Exploration of structural topologies in

metal-organic frameworks based on 3-(4-carboxyphenyl)propionic acid, their synthesis, sorption, and luminescent property studies," *Cryst. Growth Des.*, vol. 14, no. 4, pp. 2022–2033, 2014, doi: 10.1021/cg500149s.

[11] P. Kanoo *et al.*, "Crystal Dynamics in Multi-stimuli-Responsive Entangled Metal–Organic Frameworks," *Chem. - A Eur. J.*, vol. 22, no. 44, pp. 15864–15873, 2016, doi: 10.1002/chem.201602087.

[12] W. S. Jeong *et al.*, "Modeling adsorption properties of structurally deformed metal–organic frameworks using structure–property map," *Proc. Natl. Acad. Sci. U. S. A.*, vol. 114, no. 30, pp. 7923–7928, 2017, doi: 10.1073/pnas.1706330114.

[13] J. S. M. Anderson, L. Massa, and C. F. Matta, "Non-Nuclear maxima and the universality of Bright Wilson's justification of the first Hohenberg Kohn theorem revisited," *Chem. Phys. Lett.*, vol. 780, no. August, 2021, doi: 10.1016/j.cplett.2021.138940.

[14] D. Nazarian, J. S. Camp, and D. S. Sholl, "A Comprehensive Set of High-Quality Point Charges for Simulations of Metal-Organic Frameworks," *Chem. Mater.*, vol. 28, no. 3, pp. 785–793, 2016, doi: 10.1021/acs.chemmater.5b03836.

[15] J. L. Mancuso, A. M. Mroz, K. N. Le, et al., "Electronic Structure Modeling of Metal-Organic Frameworks," *Chem. Rev.*, vol. 120, no. 16, pp. 8641–8715, 2020, doi: 10.1021/acs.chemrev.0c00148.

[16] C. G. Piscopo and S. Loebbecke, "Strategies to Enhance Carbon Dioxide Capture in Metal-Organic Frameworks," *Chempluschem*, vol. 85, no. 3, pp. 538–547, 2020, doi: 10.1002/cplu.202000072.

[17] J. Liu, P. K. Thallapally, B. P. Mc Grail, et al., "Progress in adsorption-based CO2 capture by metal–organic frameworks," *Chem. Soc. Rev.*, vol. 41, no. 6, pp. 2308–2322, 2012, doi: 10.1039/c1cs15221a.

[18] Q. Zhao, Z. Ren, P. Zhao, et al., "Exact-exchange relativistic density functional theory in three-dimensional coordinate space," *Phys. Lett. Sect. B Nucl. Elem. Part. High-Energy Phys.*, vol. 860, no. December 2024, p. 139196, 2025, doi: 10.1016/j.physletb.2024.139196.

[19] D. W. Keith, G. Holmes, D. St. Angelo, et al., "A Process for Capturing CO2 from the Atmosphere," *Joule*, vol. 2, no. 8, pp. 1573–1594, 2020, doi: 10.1016/j.joule.2018.05.006.

[20] N. S. Bobbitt *et al.*, "MOFX-DB: An Online Database of Computational Adsorption Data for Nanoporous Materials," *J. Chem. Eng. Data*, vol. 68, no. 2, pp. 483–498, Feb. 2023, doi: 10.1021/acs.jced.2c00583.

[21] C. Xue, T. Zhang, and D. Xiao, "Output related fault detection and diagnosis based on multi block modified orthogonal Broyden-Fletcher-Goldfarb-Shanno algorithm," *Neurocomputing*, vol. 607, no. 3, p. 128350, 2024, doi: 10.1016/j.neucom.2024.128350.

[22] H. Zhang *et al.*, "Advanced orthogonal moth flame optimization with Broyden–Fletcher–Goldfarb–Shanno algorithm: Framework and real-world problems," *Expert Syst. Appl.*, vol. 159, 2020, doi: 10.1016/j.eswa.2020.113617.

[23] D. Jadav *et al.*, "Mesoporous silica supported ionic liquid materials with high efficacy for CO2 adsorption studies," *J. Ion. Liq.*, vol. 4, no. 2, p. 100102, 2024, doi: 10.1016/j.jil.2024.100102.

[24] J. M. Rimsza and T. M. Nenoff, "Critical role of solvation on CC13 porous organic cages for design of porous liquids," *J. Mol. Liq.*, vol. 401, no. April, p. 124731, 2024, doi: 10.1016/j.molliq.2024.124731.

[25] A. Nalaparaju, M. Khurana, S. Farooq, et al., "CO_2 capture in cation-exchanged metal-organic frameworks: Holistic modeling from molecular simulation to process optimization," *Chem. Eng. Sci.*, vol. 124, pp. 70–78, 2015, doi:

10.1016/j.ces.2014.09.054.
[26] I. Majchrzak-Kucęba and D. Bukalak-Gaik, "Regeneration performance of metal–organic frameworks: TG-Vacuum tests," *J. Therm. Anal. Calorim.*, vol. 125, no. 3, pp. 1461–1466, 2016, doi: 10.1007/s10973-016-5624-2.
[27] X. Guo, Z. Zhou, C. Chen, et al., "New rht-Type Metal−Organic Frameworks Decorated with Acylamide Groups for Efficient Carbon Dioxide Capture and Chemical Fixation from Raw Power Plant Flue Gas," *ACS Appl. Mater. Interfaces*, vol. 8, no. 46, pp. 31746–31756, 2016, doi: 10.1021/acsami.6b13928.
[28] D. Wang *et al.*, "Enhancing reversibility of LiNi0.5Mn1.5O4 by regulating surface oxygen deficiency," *Carbon Energy*, vol. 5, no. 11, pp. 1–9, 2023, doi: 10.1002/cey2.338.
[29] H. Kang *et al.*, "Enhancing CO2 Reduction Efficiency on Cobalt Phthalocyanine via Axial Ligation," *ChemCatChem*, vol. 15, no. 14, 2023, doi: 10.1002/cctc.202300576.
[30] A. S. Morshedy, H. M. Abd El Salam, A. M. A. El Naggar, et al., "Hydrogen Production and in Situ Storage through Process of Water Splitting Using Mono/Binary Metal-Organic Framework (MOF) Structures as New Chief Photocatalysts," *Energy and Fuels*, vol. 34, no. 9, pp. 11660–11669, 2020, doi: 10.1021/acs.energyfuels.0c01559.
[31] J. Du *et al.*, "Hard-and-Soft Integration Strategy for Preparation of Exceptionally Stable Zr(Hf)-UiO-66 via Thiol-Ene Click Chemistry," *ACS Appl. Mater. Interfaces*, vol. 12, no. 25, pp. 28576–28585, 2020, doi: 10.1021/acsami.0c10368.
[32] F. Giorgi *et al.*, "The influence of inter-particle forces on diffusion at the nanoscale," *Sci. Rep.*, vol. 9, no. 1, pp. 1–6, 2019, doi: 10.1038/s41598-019-48754-5.
[33] S. Katnagallu *et al.*, "Impact of local electrostatic field rearrangement on field ionization," *J. Phys. D. Appl. Phys.*, vol. 51, no. 10, 2018, doi: 10.1088/1361-6463/aaaba6.
[34] K. Zhang, H. Liu, M. Ma, et al., "Multiscale Fractal Characterization of Pore–Fracture Structure of Tectonically Deformed Coal Compared to Primary Undeformed Coal: Implications for CO2 Geological Sequestration in Coal Seams," *Processes*, vol. 11, no. 10, 2023, doi: 10.3390/pr11102934.
[35] L. Kulakova, G. Arampatzis, P. Angelikopoulos, et al., "Data driven inference for the repulsive exponent of the Lennard-Jones potential in molecular dynamics simulations," *Sci. Rep.*, vol. 7, no. 1, pp. 1–10, 2017, doi: 10.1038/s41598-017-16314-4.
[36] N. Inui, "Equilibrium shape of a suspended graphene sheet under electrostatic and van der Waals forces," *J. Phys. D. Appl. Phys.*, vol. 51, no. 11, 2018, doi: 10.1088/1361-6463/aaad9b.
[37] S. Kawai *et al.*, "Extended halogen bonding between fully fluorinated aromatic molecules," *ACS Nano*, vol. 9, no. 3, pp. 2574–2583, 2015, doi: 10.1021/nn505876n.
[38] S. Hamad, S. R. G. Balestra, R. Bueno-Perez, et al., "Atomic charges for modeling metal-organic frameworks: Why and how," *J. Solid State Chem.*, vol. 223, pp. 144–151, 2015, doi: 10.1016/j.jssc.2014.08.004.
[39] M. K. Taylor *et al.*, "Tuning the Adsorption-Induced Phase Change in the Flexible Metal-Organic Framework Co(bdp)," *J. Am. Chem. Soc.*, vol. 138, no. 45, pp. 15019–15026, 2016, doi: 10.1021/jacs.6b09155.